2022 IEEE 5th International Conference on Soft Robotics (RoboSoft)
April 4-8, 2022, Edinburgh, UK

Design and Fabrication of 3D Papercraft IPMC Robots

Hiroyuki Nabae[1], Keita Kubo[1], Kazuki Shishikura[1],
Tetsuya Horiuchi[2], Kinji Asaka[2], Gen Endo[1], and Koichi Suzumori[1]

***Abstract*— Ionic-polymer metal composites (IPMC) actuators, which are typical polymer gel actuators, can be driven at a low voltage and provide high responsiveness and large displacement. Conventional robots using IPMC actuators were generally fabricated by cutting and pasting sheet-shaped IPMCs, which posed a problem in realizing complex three-dimensional (3D) shapes and motions. To address this problem, we previously proposed a fabrication method (Simultaneous 3D Forming and Patterning, SFP) that simultaneously achieves a 3D shape using the shape memory property of the ion-exchange membrane and segments the IPMCs by masking with a jig. However, the shapes that can be formed by SFP method are limited to those that can be formed just by bending the sheets, which should be extended to more complicated shapes of IPMCs. Therefore, in this paper, we propose a new type of 3D IPMC robots inspired by papercrafts that can form their shapes like "papercrafts" with a combination of SFP process and a clinching method in joining. Clinching for the ion-exchange membrane enables joining adjacent surfaces of thin-walled IPMC robots, allowing the fabrication of IPMC robots like papercrafts. After clarifying the joint strength of clinching for ion-exchange membrane, two turtle-shaped papercraft IPMC robots were designed and prototyped in two different sizes, which have highly complex 3D shapes. The prototype robots achieved the designed shapes and succeeded in the fundamental driving experiments.**

I. INTRODUCTION

In recent years, polymeric actuators have attracted considerable research attention owing to their ability to operate in a flexible, energy-saving, biological manner. One typical polymer actuator, the ionic polymer-metal composites (IPMC) actuator, is structured such that an ion-exchange membrane and a metal electrode are joined [1]. When a voltage is applied to the surface electrode, it bends towards the anode [2](Fig. 1). IPMC actuators can be driven at a low voltage (less than 5 V), with high response speeds (within 0.1 s) and a large displacement (90-degree bending angle) [3]. Moreover, they do not produce noise and can operate under water [4] [5]. Therefore, biomimetic robots, such as fish-like and snake-like robots, have been developed using IPMC actuator [6]–[8]. Conventionally developed soft IPMC robots are fabricated mainly by cutting and pasting a commercially available sheet-shaped IPMC. This assembly process is required to achieve complicated three-dimensional (3D) operations. In latest research, 3D-printed IPMC robots have been developed [9], [10]. 3D-printing made it easy to fabricate 3D shapes, but it is not suitable for the fabrication of thin-walled shapes and microstructures. Patterning the surface electrodes enables multi-degree-of-freedom in an IPMC actuator [11], [12]. But there have been no examples of fabricating complex shape electrodes on 3D surfaces.

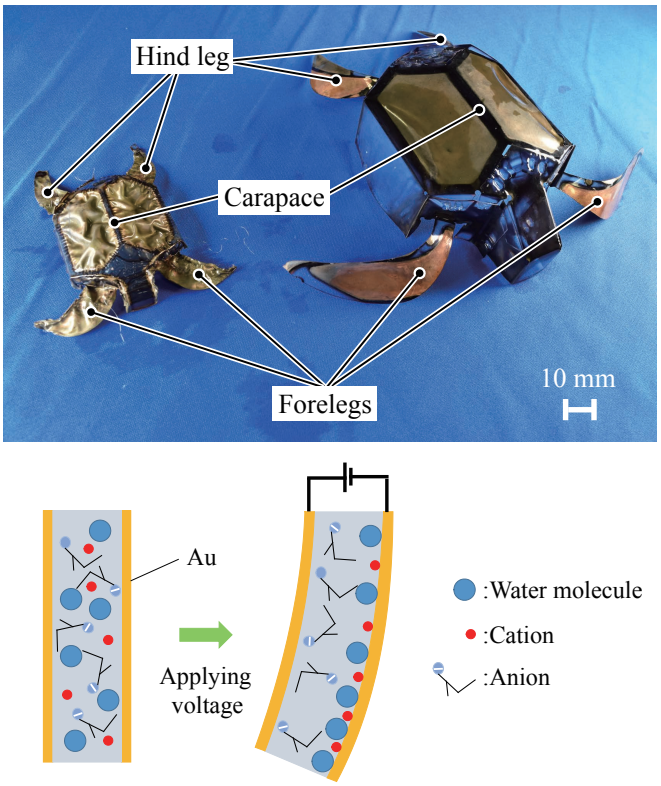

Fig. 1. Prototypes of turtle-shaped papercraft IPMC robots in two defferent sizes and schematics of driving principles of segmented IPMC actuators.

Therefore, we proposed the simultaneous 3D forming and patterning (SFP) process [13] to fabricate IPMC robots, which have a more complicated 3D shape and actuation. The SFP process utilizes jig masking and the shape memory property of the ion-exchange membrane [14]. This makes it possible to fabricate IPMC robots with 3D shapes and pattern surface electrodes on 3D surfaces. However, the only shapes that could be fabricated through the SFP process were those that could be fabricated by bending sheets. To realize more complex 3D shape IPMC robots through the

This work was supported by a Grant-in-Aid for Scientific Research in Innovative Areas under the "Science of Soft Robots" project funded by JSPS, grant number 18H05470.

[1]K. Kubo, H. Nabae, G. Endo, and K. Suzumori are with the School of Engineering, Tokyo Institute of Technology, 2-12-1 Ookayama, Meguro-ku, Tokyo 152-8550, Japan.

[2]T. Horiuchi and K. Asaka are with the National Institute of Advanced Industrial Science and Technology, Osaka 563-8577, Japan.

2022 IEEE 5th International Conference on Soft Robotics (RoboSoft) | 978-1-6654-0828-8/22/$31.00 ©2022 IEEE | DOI: 10.1109/ROBOSOFT54090.2022.9762212

SFP process, we focus on papercrafts, which can achieve complex shapes by bending and joining papers. For applying a papercraft approach to IPMC robots, the SFP process should be combined with an appropriate joining method.

Herein, this paper proposes a new type of 3D IPMC robot fabricated like papercrafts with a combination of the SFP process and a clinching method. First, the SFP process is extended to have a clinching function as a preparation for papercrafts IPMC robots, and fundamental experiments characterize its joining capacity. A design method for the proposed IPMC robots is demonstrated through prototyping two types of turtle-shaped IPMC robots (Fig. 1) that are different in size. Driving experiments are finally conducted in order to evaluate the actuation performances of the prototypes and investigate the scalability of the proposed robots.

II. 3D PAPERCRAFT IPMC ROBOT AND ITS FABRICATION PROCESS

A. 3D IPMC robot and papercraft modeling

When forming thin-walled 3D structures, the free ends are located at various parts in the body when the polyhedral shape is fabricated by bending a membrane. In the case of IPMC robot, only the shape memory property of the ion-exchange membrane can keep the shape of the robot, making it difficult to maintain its own structure. Papercraft creations overcome the aforementioned challenges by joining adjacent surfaces adding to cutting, folding, and bending. To applying the SFP process to creating 3D IPMC robots like papercrafts, the process should be extended because procedures such as cutting, bending, and molding are included in the SFP process, but adhesion has not been realized. In the case of the papercrafts, glue is applied to the glue allowance, and the adjacent surfaces are joined. Since the SFP process performs shape memory in water, join must be processed in water. However, the moisture curing adhesives weakly adhere to the ion-exchange membrane, which is a fluorinated resin. In addition, when the adhesive is cured, it is harder than the ion-exchange membrane, making it more susceptible to impact. On the other hand, thin ion-exchange membranes can easily crack and fracture if there is a notch with a small radius of curvature. Therefore, a joining technique such as a needleless stapler in which the other side is inserted into a slit on one side, is not suitable. This paper focuses on clinching, a joining method for thin metal plates. In this method, overlapping metal plates are deformed by a punch and die [15]. We propose a mechanical joining method that utilizes the shape memory property of ion-exchange membranes by applying clinching. The clinching for ion-exchange membranes differs from the original process in that heat is applied to utilize the shape memory characteristics of the ion-exchange membranes, whereas clinching is a cold process(Fig. 2). The clinching of ion-exchange membranes has the advantage that even if the joint is peeled off, it can be rejoined by pushing the concavo-convex shapes by hand again. This means that the jig that supports the IPMC robot from the inside, which is necessary when fabricating a closed structure, can be removed by peeling off the bond after molding and then rejoined. This makes maintenance tasks (e.g., placing driving circuit) easier. In addition, in the case of adhesion, the adhesive intervenes between the two ion-exchange membranes, preventing the movement of cations, but in the case of clinching of ion-exchange membranes, cations can move through the joint, so the joint can be used as an actuator or sensor by plating.

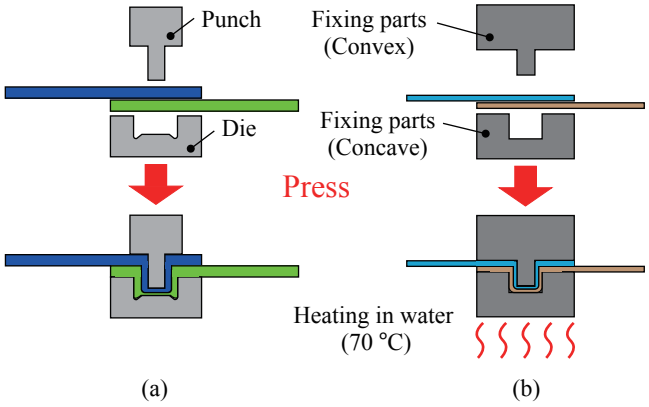

Fig. 2. Schematics of clinching: (a) original clinching (b) clinching for ion-exchange membranes.

B. Fabrication process for 3D papercraft IPMC robot

The fabrication process is divided into 3D modeling, net making, membrane formation, fixing, electroless plating, and forming processes. The flowchart is presented in Fig. 3.

1) 3D modeling process: First of all, a 3D model of a robot or masks is made by 3D CAD software.

2) Net drawing process: The drawing of the net is obtained from the 3D model in the previous process. Since the ion-exchange membrane is low in tear strength, a hole is provided at the sharp corner to reduce the stress concentration. Areas of bonding allowance are added to the net in this process in order to join the surfaces by clinching.

3) Membrane formation process: The membrane formation process involves ion-exchange membranes (Nafion™ in this study) fabrication in the net of the desired 3D shape, as shown in Fig. 6. Herein, we cut a commercially available ion-exchange membrane. An important point in the membrane formation process is that the size of the membrane must be reduced by approximately 10% to account for the expansion of the ion-exchange membrane when it absorbs water.

4) Fixing process: The fixing process is divided into the following five steps:

i) Fabricate fixation/masking jigs made of polyacetal.
ii) Soak the Nafion™ membrane in deionized water and pre-swell.
iii) Place the Nafion™ membrane on the base jig and sandwich it between the other jigs.
iv) Fix the jigs and the Nafion™ membrane using PEEK screws temporary.

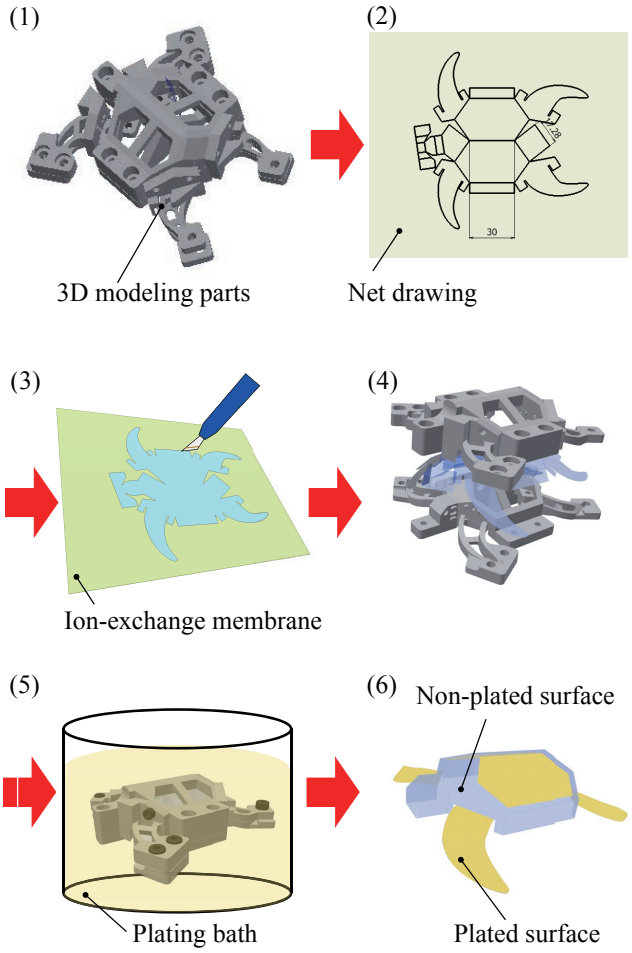

Fig. 3. Fabrication process: (1) 3D solid model for IPMC robot; (2) making net from the 3D solid model (3) membrane formation process; (4) fixing process of the SFP method; (5) electroless plating and forming process; (6) completion of IPMC robot.

v) Heat to 70 °C in deionized water and fully tighten the screws.

Fixation/masking jigs should be designed in a form that fits the desired shape of the robot. The area where the surface electrode is to be fabricated should be designed so that the jig does not touch the ion-exchange membrane and, as far as possible, interfere with the convection of the plating solution. Since ion-exchange membranes soften when they are heated to 70 °C, the clinching parts do not break. The second process is an important one. As mentioned earlier, the ion-exchange membrane expands by 10-15% when it contains liquid. Since the solvent for the plating solution is deionized water, designing a jig based on the dimensions of the ion-exchange membrane when dry will cause the ion-exchange membrane to expand and lose its shape. Therefore, the ion-exchange membrane is soaked in deionized water to expand it. Then the jig corresponding to the expanded dimensions is used to fix the membrane.

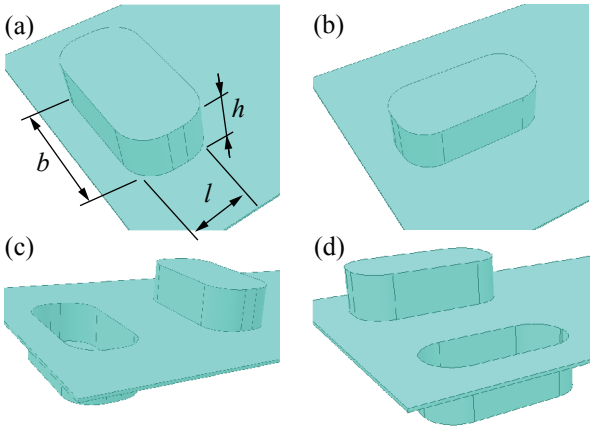

Fig. 4. Schematic diagram of the 4 out of 7 joint shape patterns and dimensional parameters for concave-convex shapes.

5) Electroless plating and forming process: The electroless gold plating process, developed by Fujiwara et al., was used to fabricate the electrodes to the Nafion™ membrane [16]. This process is divided into the following three steps:

i) Nafion™ membrane fixed with fixation/masking jigs is immersed overnight in a gold complex aqueous solution at 20 – 25 °C such that it adsorbs the gold complex ($Au[(phen)Cl_2]Cl$ aq).
ii) Soak in a reducing agent solution (Na_2SO_3 aq) at 60 °C for 3.5 h to deposit the gold on the surface.
iii) Wash membrane by immersing it in deionized water at 70 °C.

This process is repeated until the surface resistance of the electrode reaches several Ω. The heating and cooling in this process results in the shape memory of the ion-exchange membrane.

C. Characterization of the clinching for ion-exchange membrane

In general, the larger the clinching area, the more difficult it is to reduce the size and complexity of the IPMC robot, leading to a decrease in design flexibility. Therefore, to investigate the shapes that can be bonded in a smaller area, we fabricated Nafion™ specimens with multiple patterns of concavo-convex shapes and measured the bonding force by applying tensile force.

In this section, we describe the mechanical joining method for the ion-exchange membrane.

1) Test pieces for joining: Joint specimens were fabricated using Nafion™ [1] N115 (Chemours Company). A total of seven joint shapes were tested, including the four patterns shown in Fig. 4 and three downsized versions of (c). The variables are width b, length l, height h, and quantity n of the concavo-convex shape. The variables of the concavo-convex shapes for each pattern are shown in Table I. The test specimens were made by partially overlapping two

[1]Nafion™ is tradmarks of Chemours Company

TABLE I: Dimensional and geometric parameters of each joint pattern.

Pattern	*b* [mm]	*l* [mm]	*h* [mm]	Quantity *n*
(a)	10	5	3	1
(b)	5	10	3	1
(c)	10	5	3	2
(d)	5	10	3	2
(e)	10	5	1.5	2
(f)	5	2.5	1.5	2
(g)	3	2	1	2

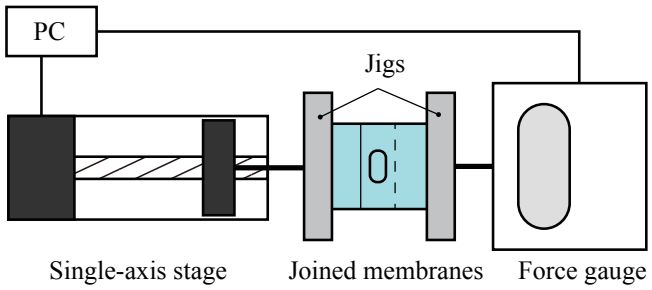

Fig. 5. Setup for measuring the joint strength of joined Nafion™ membranes.

Nafion™ membranes cut into strips of 20 $[\mathrm{mm}]$ width and 60 $[\mathrm{mm}]$ length, and clinching the ion-exchange membranes together. Patterns (a) to (d) are patterns with the same size of concavo-convex shapes, but with different numbers and arrangements. Patterns (e)-(g) are based on pattern (c), but the dimensions of the concave-convex shape are reduced to reduce the joint size. We also prepared specimens (a') and (b'), bonded with underwater adhesives for comparison experiments. The specimens were bonded by (a') applying epoxy adhesive (E380, Konishi Co., Ltd.) with 270 $[\mathrm{mm}^2]$ and (b') epoxy and amine adhesive (HermeSteel, Sannou Kogyo Co., Ltd.) with 380 $[\mathrm{mm}^2]$.

2) Test results: The test was performed using a force gauge (FGP-50, SHIMPO) and a single axis stage (PM80B-50X, COMS) to measure the joint force as shown in Fig. 5. Both ends of the specimen are fixed with a jig and connected to a force gauge and a single axis stage. The tensile force is applied by quasi-statically moving the single axis stage upward in the figure, and the applied force is recorded on a PC. The value of the tensile force just before the joint was peeled off was defined as the joint force $P_{\max}$ [N]. The joint strength $\tau_{\max}$ [MPa] is defined as the bond force divided by the area of the joint $A = b \times l \times n$ $[\mathrm{mm}^2]$.

$$\tau_{\max} = \frac{P_{\max}}{A} \tag{1}$$

The test results are shown in Table II. The number of measurement trials was three, and the values of the joint forces are the average of the maximum values of the forces measured in each experiment. The reason for the high joint strength of pattern (c) is discussed in terms of the mode in which the joint is peeled off. During the test, as the tensile force increased, the edge of the membrane was lifted up. This may be due to the rotational moment applied to the

TABLE II: Joint force and joint strength of each joint pattern.

Pattern	Joint force $P_{\max}$ [N]	Joint strength $\tau_{\max}$ [MPa]
(a)	0.63	1.2×10^{-2}
(b)	0.90	1.8×10^{-2}
(c)	3.0	3.0×10^{-2}
(d)	1.2	1.2×10^{-2}
(e)	1.1	1.1×10^{-2}
(f)	1.4	5.6×10^{-2}
(g)	1.0	8.3×10^{-2}
(a')	12.9	4.76×10^{-2}
(b')	18.0	4.67×10^{-2}

concave and convex shapes by the tensile force applied to the joint. Since the surface of the lower convex shape that receives the force from the upper convex shape is on the root side, it is thought that the entire convex shape rotates counterclockwise without deforming. The counterclockwise moment is balanced by the static friction force of the membrane and the moment due to the drag force from the upper convex shape. On the other hand, the upper convex shape is deflected by the tensile force in addition to the moment. This deflection causes the surface that receives the force from the lower convex shape to tilt, which decreases the friction force and causes the joint to peel. In short, the smaller the rotational stiffness of the joint and the smaller the moment generated, the larger the joint force. Although the rotational stiffness of (d) is higher than that of (c), the joint strength is considered to be lower because of the new moment in the plane perpendicular to the tensile direction. From the above, pattern (c) is considered to have high joint strength. Further, we describe patterns (e), (f), and (g), which are based on pattern (c) with reduced shape dimensions. Consequently, compared with pattern (d), pattern (f), in which h is half the size, has a larger joint force than pattern (d), in which all dimensions are half the size. This suggests that there is an optimal value of h for each of b and l. Pattern (g) is the smallest pattern among the patterns we fabricated. In the case of pattern (g), a joint force of 1.0 N, which is larger than the force generated by the IPMC actuator (several tens of $[\mathrm{mN}]$), was obtained.

Compared to clinching, underwater adhesives demonstrated large joint force. This is because the area of the bonded part is larger than that of the clinched part. A comparison of the joint strength shows that the joint strength of clinching is equivalent to 20-180% of that of bonding, indicating that clinching for ion-exchange membrane has sufficient strength in tension.

III. DESIGN AND PROTOTYPING OF TURTLE SHAPED IPMC ROBOT

In this section, two types of papercraft IPMC robots (large and small types) are designed and prototyped by the SFP process updated with the proposed clinching for ion-exchange membrane. The prototypes are evaluated through fundamental driving experiments and a swimming experiment in view of the scalability of the proposed process and robot.

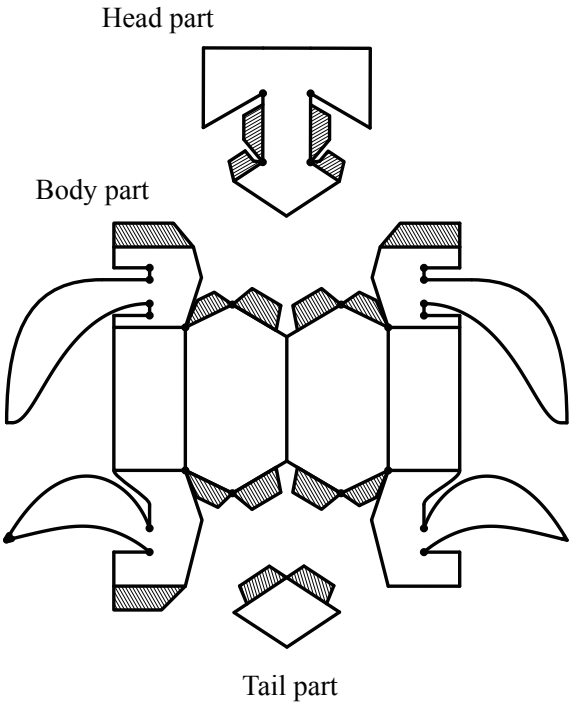

Fig. 6. Net of turtle-shaped papercraft IPMC robot (large type). Hatched area is joint allowance for clinching.

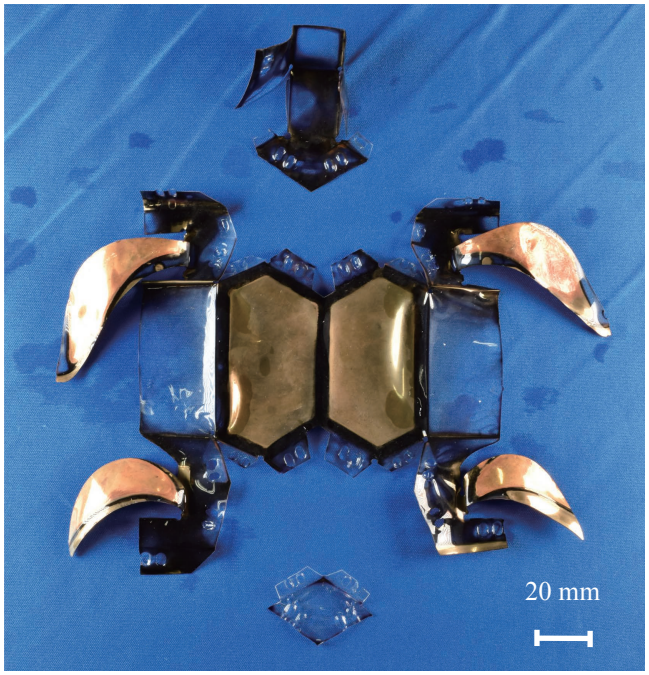

Fig. 7. IPMC sheets before constructing 3D structure (large type)

A. Prototypes of papercraft IPMC robots

The papercraft IPMC robots are fabricated by bending and joining ion-exchange membranes like a papercraft. Therefore, we first design nets of the desired 3D shape, and Fig. 6 shows the net of the large type. Since the tear strength of the ion-exchange membrane is low, as described above, holes with a radius of 2 $[\mathrm{mm}]$ are provided at the sharp corners to reduce stress concentration. The hatched area in the net of the turtle-shaped papercraft IPMC robot is the joint allowance, which overlaps the structural part. This must be added in addition to the shape of the original net. This area is joined using clinching for ion-exchange membranes. The next step is to design the fixation/masking jig according to the desired 3D shape. The fixation/masking jigs are aligned to sandwich the ion-exchange membrane from both sides. It also has a masking role to segment the IPMC, and the masking part is designed to adhere to the ion-exchange membrane. Fig. 7 shows the IPMC sheets for the large type before attaching the joint allowance. The figure indicates that the process was completed as we expected, and the hatched areas in Fig. 6 have concavo-convex structures for the clinching. The turtle-shaped IPMC robots and the fixation and masking jigs used are shown in Fig. 8. The large type and small type prototypes are made of Nafion™ N117 (183 μm in thickness) and Nafion™ N115 (127 μm in thickness), respectively. In the turtle shaped IPMC robots, the body and head are the main structural parts, and the forelegs, hind legs, and a part of the carapace are actuators. Moreover, the 3D structure of carapace helps to stabilize the robot's posture on the water surface. However, since the carapace was not completely sealed, it could not float on its own, so this time we used styrofoam to provide buoyancy.In addition, the tummy side is not closed. In this study, the actuator parts of four segments of the forelegs and hindlegs were clamped with clip electrodes to apply voltage. The actuator parts of the carapace were not used.

B. Driving experiments

1) Test operation and measurement resonant frequency: Two turtle-shaped IPMC robots were tested by applying voltage to each of their four legs using clip electrodes. Further, to measure the resonance frequency of each leg, the displacement of the tip of each leg was measured using a laser displacement meter(LK-G32, KEYENCE CORPORATION) when a sinusoidal voltage of $1\ [\mathrm{V}], 0.1-50\ [\mathrm{Hz}]$ was applied. The motion of the large type leg is shown in Fig. 9, and the results of the frequency responses are shown in Fig. 10.

Apparent resonant frequency can not be observed from the result of Fig. 10(a). It would come from the high damping ratio of the actuation part of the prototype. The results of Fig. 10(b) show almost same tendencies as Fig. 10(a). Although a profile of left foreleg in Fig. 10(b) has a peak around 8 Hz, the other legs indicate no apparent peaks. Because the gain values were calculated with the ratio of amplitudes in the output displacement and input voltage, the higher gain in Fig. 10(b) than in Fig. 10(a) means the larger displacement of the large prototype.

2) Swimming experiment: In the motion experiment, only the right hind leg was clamped to perform the swimming experiment because the stiffness of the wiring may interfere with the motion of the turtle-shaped papercraft IPMC robot.

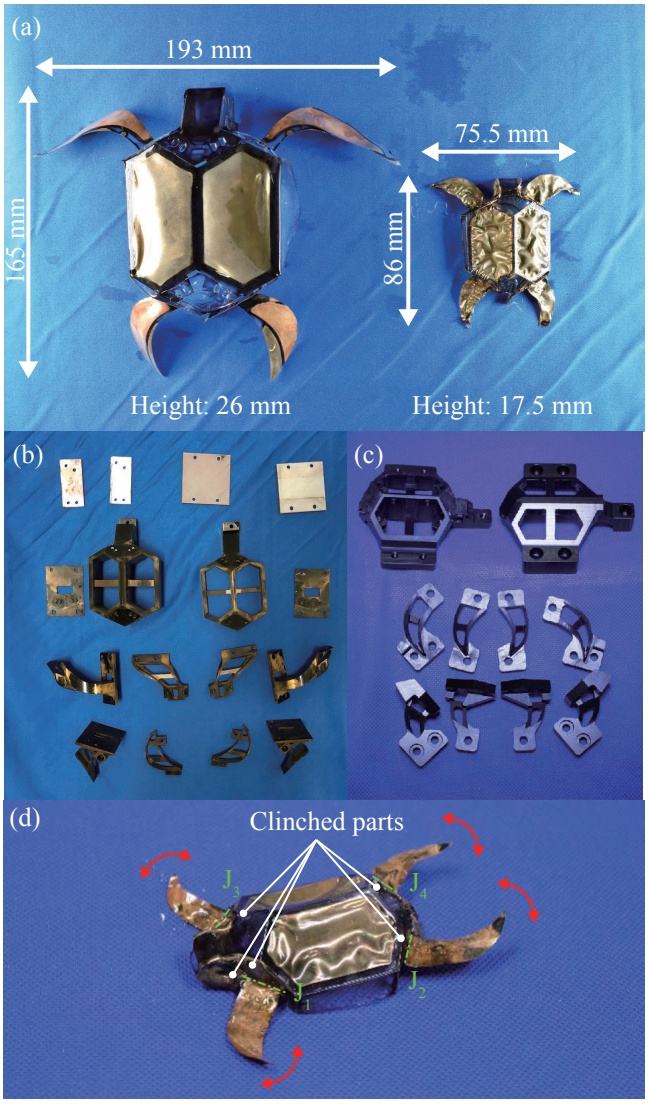

Fig. 8. Photograph of turtle-shaped IPMC robot and fixing/masking jigs: (a) top view of smaller turtle-shaped papercraft IPMC robot (b) fixation/masking jigs of (a) (c) top view of the large turtle-shaped papercraft IPMC robot (d) fixation/masking jigs of (c) (e) clinchied parts in the body, joints of each leg, and movement of actuator parts.

The experiment is conducted in deionized water as shown inFig. 11. When a voltage of 8 [V], 7 [Hz] was applied to the right hind paw of the small prototype, it was confirmed to move forward at a speed of 1.95 [mm/s] while the large prototype failed in the swimming operation.

Although the right hind leg drives in the maximum motion amplitude at 0.6 [Hz], the robot did not move when a sinusoidal voltage of 0.6 [Hz] was applied. IPMC actuator is expected to decrease the generated force due to its own stiffness as the displacement increases. Therefore, using the driving frequency of the IPMC to obtain the maximum displacement is not always optimal for the turtle-shaped papercraft IPMC robot. Regarding the large prototype, enough thrust force could not be obtained even when the legs were moved by

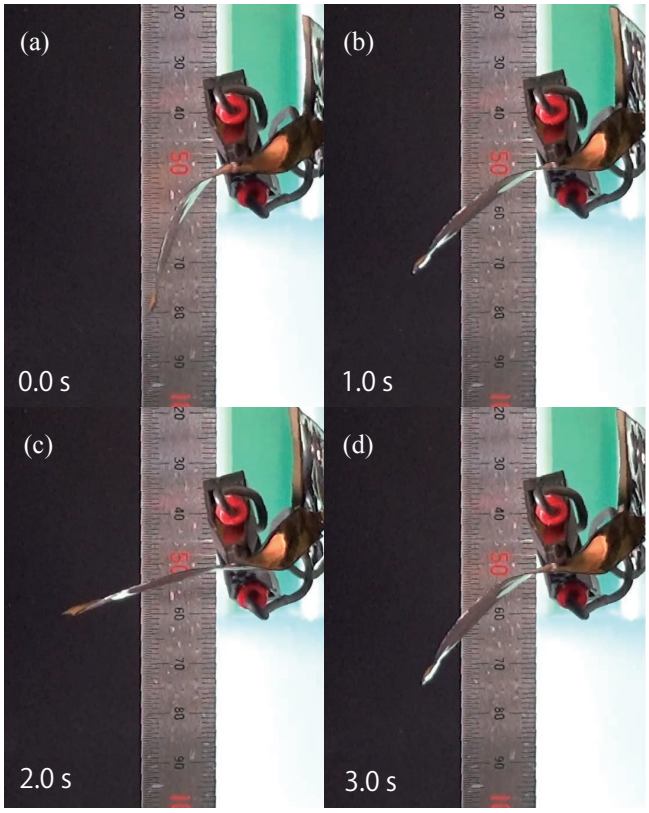

Fig. 9. Leg motion of the large prototype.

changing the frequency. Assuming the generated force is proportional to the bending stiffness, it is proportional to the cube of the length, while the drag force due to water is proportional to the square of the length because it is related to the representative area. This discussion implies that the proposed robot, which has a relatively small hydraulic force owing to consisting of thin films, has a disadvantage in the larger size for the swimming experiments.

IV. DISCUSSION

In this section, we first disscuss the clinching joint strength of ion-exchange membranes mainly focusing on four shape patterns. The number of samples was insufficient to formulate the bonding force obtained, and qualitative discussions were limited. To clarify the joint mechanism in the future, a large number of patterns must be fabricated and formulated experimentally.

We used Nafion™ membranes cut out as a membrane formation method to fabricate the IPMC robot. In the future, we plan to use Nafion™ membranes of different thickness formed by the multi-layer casting process [17]. This will help us realize a more flexible 3D paper craft IPMC robot by enabling the design of thicker structural parts and thinner driving parts of the robot.

The turtle-shaped paper craft IPMC robot also has two segmented actuators in the carapace, but they were not used in the experiment. We are currently investigating a method to obtain the electrical conductivity between the surface

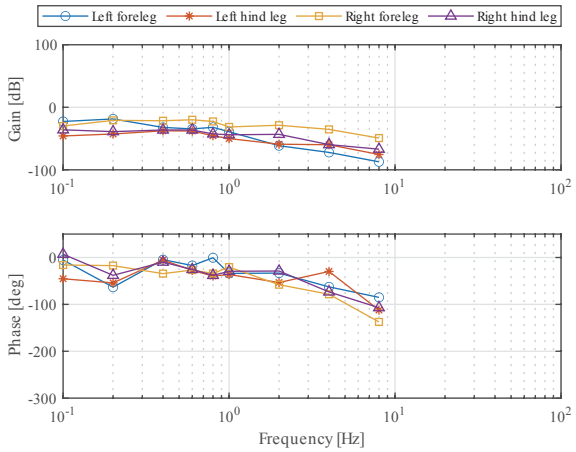

(a) Small type

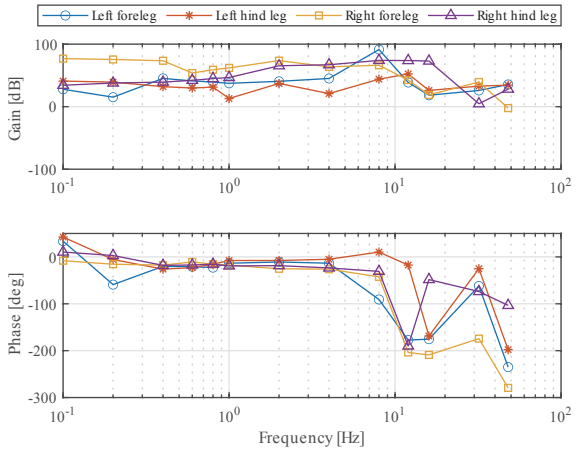

(b) Large type

Fig. 10. Bode diagrams of each leg of turtle-shaped papercraft IPMC robots.

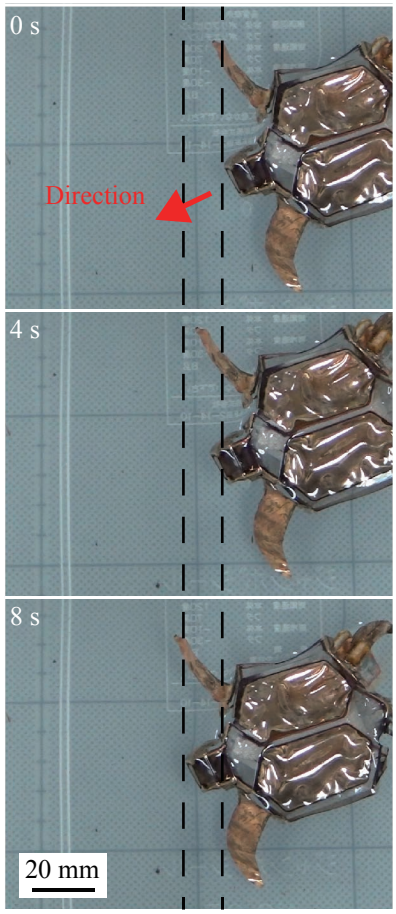

Fig. 11. The turtle-type papercraft IPMC robot moving forward in a swimming experiment.

electrodes of the IPMC and the external drive circuit. If this problem can be solved, it will be possible to realize levitation and descent by driving the actuator part of the carapace. Furthermore,the papercraft IPMC robot joined by clinching can be detached and rejoined, making it easy to install drive circuits and batteries inside. And it is expected to achieve independent operation.

V. CONCLUSION

In this paper, we propose a new type of 3D IPMC robot that can be constructed like papercrafts. The SFP process was extended to have the function of joining adjacent surfaces by clinching to realize the proposed IPMC robot. The clinching for ion-exchange membranes is evaluated by the fundamental experiments. The joint force of the clinched Nafion™ membranes is 1.0 [N] even for the smallest shape among the patterns fabricated, which is sufficiently larger than the force generated by IPMC (several tens of [mN]) to prevent the robot from self-destructing owing to its own generated force. In addition, depending on the pattern, the bonding strength was comparable to that of underwater adhesives. After the explanation of the proposed design and fabrication method, two types of turtle-shaped IPMC robots were prototyped to demonstrate the design method and fabrication process of the 3D papercraft IPMC robot. Driving experiments are finally conducted in order to demonstrate actuation performances of the prototypes and investigate the scalability of the proposed robots. We succeeded in forming the highly complex 3D structure in the two sizes of prototypes and driving the legs. The frequency responses of the two prototypes show almost the same tendency in the curve profiles, but the effect of scale can be observed in the gain value and cut-off frequencies. In swimming experiments, we achieved forward motion at 1.95 [mm/s] by the small type. Those results successfully show the applicability of the proposed concept to practical IPMC robots and the potential for enhancing the field of IPMC applications.

REFERENCES

[1] K. Oguro, Y. Kawami, and H. Takenaka, "Bending of an ion-conducting polymer film-electrode composite by an electric stimulus at low voltage," *J. Micromachine Society*, vol. 5, pp. 27–30, 1992.

[2] S. Nemat-Nasser and J. Y. Li, "Electromechanical response of ionic polymer-metal composites," *Journal of Applied Physics*,

vol. 87, no. 7, pp. 3321–3331, 2000. [Online]. Available: https://doi.org/10.1063/1.372343

[3] M. Konyo and S. Tadokoro, *IPMC Based Tactile Displays for Pressure and Texture Presentation on a Human Finger*. John Wiley and Sons, Ltd, 2009, ch. 8, pp. 161–174. [Online]. Available: https://onlinelibrary.wiley.com/doi/abs/10.1002/9780470744697.ch8

[4] D. Pugal, K. Jung, A. Aabloo, and K. J. Kim, "Ionic polymer-metal composite mechanoelectrical transduction: review and perspectives," *Polymer International*, vol. 59, no. 3, pp. 279–289, Mar 2010. [Online]. Available: https://doi.org/10.1002/pi.2759

[5] K. Jung, J. Nam, and H. Choi, "Investigations on actuation characteristics of ipmc artificial muscle actuator," *Sensors and Actuators A: Physical*, vol. 107, no. 2, pp. 183 – 192, 2003. [Online]. Available: http://www.sciencedirect.com/science/article/pii/S0924424703003467

[6] B. L. Stoimenov, J. Rossiter, and T. Mukai, "Soft ionic polymer metal composite (IPMC) robot swimming in viscous fluid," in *Electroactive Polymer Actuators and Devices (EAPAD) 2009*, Y. Bar-Cohen and T. Wallmersperger, Eds., vol. 7287, International Society for Optics and Photonics. SPIE, 2009, pp. 757 – 764. [Online]. Available: https://doi.org/10.1117/12.818705

[7] M. Yamakita, N. Kamamichi, T. Kozuki, K. Asaka, and Zhi-Wei Luo, "A snake-like swimming robot using ipmc actuator and verification of doping effect," in *2005 IEEE/RSJ International Conference on Intelligent Robots and Systems*, Aug 2005, pp. 2035–2040.

[8] X. Ye, Y. Su, and S. Guo, "A centimeter-scale autonomous robotic fish actuated by ipmc actuator," in *2007 IEEE International Conference on Robotics and Biomimetics (ROBIO)*, Dec 2007, pp. 262–267.

[9] J. D. Carrico, K. J. Kim, and K. K. Leang, "3d-printed ionic polymer-metal composite soft crawling robot," in *2017 IEEE International Conference on Robotics and Automation (ICRA)*, May 2017, pp. 4313–4320.

[10] H. Nabae, A. Ishiki, T. Horiuchi, K. Asaka, G. Endo, and K. Suzumori, "Frequency response of honeycomb structured ipmc actuator fabricated through 3d printing with dispersion liquid," in *2019 International Symposium on Micro-NanoMechatronics and Human Science (MHS)*. IEEE, 2019, pp. 1–3.

[11] Y. Nakabo, T. Mukai, and K. Asaka, "Biomimetic soft robots with artificial muscles," in *Smart Materials III*, A. R. Wilson, Ed., vol. 5648, International Society for Optics and Photonics. SPIE, 2004, pp. 132 – 144. [Online]. Available: https://doi.org/10.1117/12.581825

[12] Y. Wang, H. Chen, Y. Wang, J. Liu, and D. Li, "Manufacturing process for patterned ipmc actuator with millimeter thickness," in *2013 IEEE International Symposium on Assembly and Manufacturing (ISAM)*, July 2013, pp. 235–239.

[13] K. Kubo, H. Nabae, T. Horiuchi, K. Asaka, G. Endo, and K. Suzumori, "Simultaneous 3d forming and patterning method of realizing soft ipmc robots," in *2020 IEEE International Conference on Intelligent Robotics and Systems (IROS)*. IEEE, Oct 2020, pp. 8815 – 8822.

[14] K. A. Mauritz and R. B. Moore, "State of understanding of nafion," *Chemical reviews*, vol. 104, no. 10, pp. 4535–4586, 2004.

[15] S.-W. Pak and S.-Y. Kwon, "Application of mechanical clinching method to aluminum hood," in *SAE Technical Paper*. SAE International, 02 1995. [Online]. Available: https://doi.org/10.4271/950714

[16] N. Fujiwara, K. Asaka, Y. Nishimura, K. Oguro, and E. Torikai, "Preparation of gold solid polymer electrolyte composites as electric stimuli-responsive materials," *Chemistry of Materials*, vol. 12, no. 6, pp. 1750–1754, 2000.

[17] A. Kodaira, K. Asaka, T. Horiuchi, G. Endo, H. Nabae, and K. Suzumori, "Ipmc monolithic thin film robots fabricated using a multi-layer casting process," *IEEE Robotics and Automation Letters*, vol. 4, pp. 1335–1342, 2019.